https://doi.org/10.5194/egusphere-2025-2696
Preprint. Discussion started: 25 June 2025

An in-situ methodology to separate the contribution of soil water content and salinity to EMI-based soil electrical conductivity

Dario Autovino[1-2], Antonio Coppola[3], Roberto De Mascellis[2], Mohammad Farzamian[4], Angelo Basile[2]

[1]Department of Agricultural, Food and Forest Sciences, University of Palermo, Palermo, 90128, Italy
[2]Institute for Mediterranean Agricultural and Forestry Systems, National Research Council of Italy, Portici, 80055, Italy
[3]Department of Chemical and Geological Sciences, University of Cagliari, Monserrato, 09042, Italy
[4]Instituto Nacional de Investigação Agrária e Veterinária, Oeiras 2780-157, Portugal

Correspondence to: Dario Autovino (dario.autovino@unipa.it)

Abstract. Salt accumulation in the root zone limits agricultural productivity and can eventually lead to land abandonment. Therefore, monitoring the spatial distribution of soil water content and solution salinity is crucial for effective land and irrigation management. However, assessing soil water content and salinity at the field scale is often challenging due to the heterogeneity of soil properties.

Electromagnetic induction (EMI) offers a fast, non-invasive, in situ geophysical method to map spatial variability in soil. EMI instruments measure the apparent soil electrical conductivity (EC_a), which reflects the integrated contribution of the bulk electrical conductivity (σ_b) of different soil layers. By inverting the measured EC_a, it is possible to obtain the distribution of the σ_b along the soil profile, which provides indirect information on soil salinity. However, in saline soils, σ_b is influenced by both water content (θ) and soil solution electrical conductivity (σ_w) (the salinity), making it difficult to independently quantify these two variables through a single, straightforward procedure.

The objective of this study is to separate the respective contributions of θ and σ_w to σ_b, as obtained from the EMI inversion. To achieve this, EC_a was measured using a CMD-MiniExplorer instrument in two maize plots irrigated with saline and non-saline water, respectively, in an agricultural field in southern Italy. The dataset was then inverted in order to obtain the σ_b distribution. By employing a site-specific calibrated Rhoades linear model and assuming homogeneity between the two plots, the spatial distribution of θ and σ_w in the saline plot was successfully estimated. To validate the results, independent measurements of soil water content by Time Domain Reflectometry (TDR) and direct measurement of soil solution electrical conductivity, σ_w, were performed.

The proposed procedure enables the estimation of θ and σ_w with high accuracy along the soil profile, except in the soil surface, where EMI reliability is limited. These findings demonstrate that the integration of EMI with a site-specific θ - σ_b - σ_w model is a reliable and efficient in-situ approach for mapping soil salinity and water content at field scale, offering valuable insights for optimizing agricultural irrigation management in systems using saline water.

https://doi.org/10.5194/egusphere-2025-2696
Preprint. Discussion started: 25 June 2025

1 Introduction

Regions with hot, dry summers are often irrigated with low-quality saline water to alleviate water scarcity (Ghazouani et al., 2015; Tlig et al., 2023). However, this practice can lead to the accumulation of soluble salts in the root zone, causing soil salinization (Brouwer et al., 1985). Salt stress occurs when the osmotic potential decreases due to the presence of soluble salts in the soil solution, which inhibits water uptake by the roots (Coppola et al., 2015; Rasool et al., 2013). Hence, soil salinization is one of the most significant abiotic stresses affecting agriculture (de Oliveira et al., 2013).

The Global Map of Salt-Affected Soils (https://www.fao.org/soils-portal/data-hub/soil-maps-and-databases/global-map-of-salt-affected-soils/ar/) indicates that salt-affected soils are widespread globally, with around two-thirds of the affected areas located in arid and semi-arid climatic zones. It is estimated that salt-affected soils cover approximately 4.4% of the topsoil (0-30 cm) and over 8.7% of the subsoil (30-100 cm) of the total land area.

Therefore, accurately assessing soil salinity and the distribution of soil water content (θ) is essential for managing irrigation with saline water while maintaining acceptable crop yields (Dragonetti et al., 2018; Selim et al., 2013). This approach helps preventing stress conditions that could limit crop productivity. The most commonly used method for evaluating soil salinity is measuring the electrical conductivity of the soil solution (σ_w) (Campbell et al., 1949). Different direct and indirect procedures can be used to measure θ and σ_w. In general, direct methods such as the gravimetric method for θ and the soil extract method for σ_w are accurate but non-reproducible and require significant effort and time for measuring θ and σ_w distribution, making them impractical in most applicative cases. Time Domain Reflectometry (TDR) is a well-established non-destructive method for measuring soil dielectric permittivity (ε) and impedance (Z). This method allows for the simultaneous estimation of both soil water content (θ) from ε and bulk electrical conductivity (σ_b) from Z (Bouksila et al., 2008; Dalton et al., 1984; Noborio, 2001). σ_b is influenced by several factors, including soil water content, electrical conductivity of the soil solution, the tortuosity of the soil-pore system, soil temperature, and other factors related to the solid phase, such as bulk density, clay content, and mineralogy (McNeill, 1980; Muñoz-Carpena et al., 2005). However, over the past few decades, both physical and empirical approaches have been developed to estimate the relationship between the three key variables that fluctuate over time: σ_w, θ, and σ_b values (Hilhorst, 2000; Malicki and Walczak, 1999; Mualem and Friedman, 1991; Nadler et al., 1984; Rhoades et al., 1976, 1989). By measuring two of the three quantities in this relationship, Time Domain Reflectometry (TDR) remains a highly effective method for monitoring soil salinity.

While TDR measurements and other direct methods offer advantages, they are limited to investigating small soil volumes at a restricted number of sites, making them suitable primarily for local-scale monitoring (Shanahan et al., 2015). In contrast, the Electromagnetic Induction (EMI) method provides fast and reliable estimations of θ and σ_b over larger spatial scales (Robinet et al., 2018). This technique employs inductive coupling and has the benefit of requiring no direct contact with the soil surface (Mester et al., 2011). Additionally, EMI enables the rapid mapping of soil variability across extensive areas with high spatial resolution (Doolittle and Brevik, 2014).

https://doi.org/10.5194/egusphere-2025-2696
Preprint. Discussion started: 25 June 2025

EMI sensors measure a depth-weighted average of apparent electrical conductivity (EC_a). To extract the distribution of σ_b along soil profiles, the EC_a values obtained by EMI sensors must be inverted using either a cumulative sensitivity approach (McNeill, 1980) or the full solution of Maxwell's equations (Mester et al., 2011). Lavoué et al. (2011) introduced a calibration technique to improve the accuracy of σ_b measurements by incorporating data from Electrical Resistivity Tomography (ERT). Alternatively, multiple TDR observations can be used as an effective substitute for ERT when monitoring the root zone (Dragonetti et al., 2018).

However, even when a reliable distribution of σ_b is obtained through the inversion of EMI-based ECa readings, distinguishing the individual contributions of water content (θ) and soil salinity (σ_w) to these σ_b values remains a challenging task. Unlike TDR, EMI does not provide simultaneous measurements of water content, necessitating the development of alternative methods to isolate the influence of θ and σ_w on the estimated σ_b. In soils where salinity is low and relatively stable, a linear relationship between θ and σ_b derived from EMI measurements can be effectively applied (Altdorff et al., 2018; Badewa et al., 2018; Brevik et al., 2006; Huang et al., 2016; Serrano et al., 2013). On the other hand, in saline soils where salt concentration is significant and varies over time and spatially, a sole σ_b measurement cannot simultaneously determine both θ and σ_w (Dragonetti et al., 2022; Farzamian et al., 2021).

This study aims to develop an EMI-based methodology for estimating the field-scale evolution of σ_w distribution in saline-irrigated soils. Specifically, it explores the potential of EMI measurements to distinguish soil water content from the bulk electrical conductivity of soil water within the EMI signal. By evaluating this approach under controlled conditions, its validity and limitations were assessed, providing a foundation for broader applications in soil monitoring and irrigation management and identifying further research needs to make the approach more feasible and relevant for precision agriculture applications.

2 Material and Methods

2.1 Field experiment

The experiment was conducted at the "Arca 2010" farm, located in Acerra municipality, approximately 20 km northeast of Naples, Italy (40°57'58" N, 14°25'47" E, 27 m a.s.l.) (see Fig. 1, top panel). The farm is situated in a flat area characterized by Mollic Vitric Andosols (IUSS Working Group WRB, 2015). This soil profile includes a topsoil layer from 0 to 40 cm and a subsoil layer from 40 to 110 cm, both with a sandy loam texture and high chemical and physical fertility (Bonfante et al., 2019). The climate is typically Mediterranean, with an average annual rainfall of 876 mm and an average temperature of 16.9°C.

Two plots of silage maize (Zea mays) were arranged in this field, each measuring 18 × 68 meters, covering a total area of 1,224 m² per plot. The maize was seeded on April 16th, with a row spacing of 0.17 m and 0.75 m between adjacent rows and harvested on August 2nd (see Fig. 1, top panel).

https://doi.org/10.5194/egusphere-2025-2696
Preprint. Discussion started: 25 June 2025

Irrigation was performed using a dripline system, consisting of thin-walled polyethylene pipes installed between adjacent plant rows. The system featured drippers spaced 10 cm apart, with a flow rate of 1.5 l h^{-1}. Throughout the growing season, both plots received six irrigation treatments, each providing 490 (±154) m^3 ha^{-1} of water on the same days.

The irrigation water for the non-saline plot had a background electrical conductivity of 1.6 dS m^{-1}. In contrast, for the saline plot, calcium chloride ($CaCl_2$) was added to achieve an electrical conductivity of approximately 8 dS m^{-1}.

During the growing season, the leaf water potential, ψ, was measured on a well expanded, fully light-exposed leaf for each plot using a Scholander type pressure bomb (SAPS II, 3115, Soilmoisture Equipment Corp., Santa Barbara CA, USA). After cutting, the leaf was promptly inserted in the pressure bomb, where pressure was increased at a rate of 0.2 MPa min^{-1} to determine ψ.

On August 2nd, after maize harvesting, apparent soil electrical conductivity (EC_a) measurements were taken on both plots using the CMD Mini-Explorer (GF Instruments, Brno, Czech Republic). This device features three receiver coils positioned at distances of 0.32 meters (ρ32), 0.71 meters (ρ71), and 1.18 meters (ρ118) from the transmitter coil, operating at a frequency of 30 kHz. We utilized two coil configurations with this probe: horizontal coplanar (HCP) and vertical coplanar (VCP) loops. In HCP mode, the instrument can probe depths of up to 1.8 meters with the largest coil spacing, whereas VCP mode allows for depth investigation up to 0.9 meters. Measurements were acquired along a 17-meter-long transect, located centrally in each plot (see Fig. 1, top panel).

On the same day, following the EMI measurements, a 17-meter trench was excavated in the saline plot to a depth of 1.4 meters, directly along the EMI transect. TDR (time-domain reflectometry) probes were inserted into 17 vertical profiles within the trench, spaced 1 meter apart and positioned at four depths (15, 50, 75, and 90 cm), resulting in a total of 68 measurement points (see Fig. 1, bottom panel). For each point, the Tektronix 1502 C cable tester was used to analyse the acquired wave, measuring the dielectric permittivity (ε) and impedance (Z) over a long time to estimate soil moisture content (θ) and bulk electrical conductivity (σ_b), respectively.

Notably, TDR measurements were performed in the same positions where time-lapse EMI measurements were previously made, so as to have reference, point-scale values of soil water content and bulk electrical conductivity. Finally, 68 undisturbed soil samples were collected in the same locations where TDR measurements were performed.

https://doi.org/10.5194/egusphere-2025-2696
Preprint. Discussion started: 25 June 2025

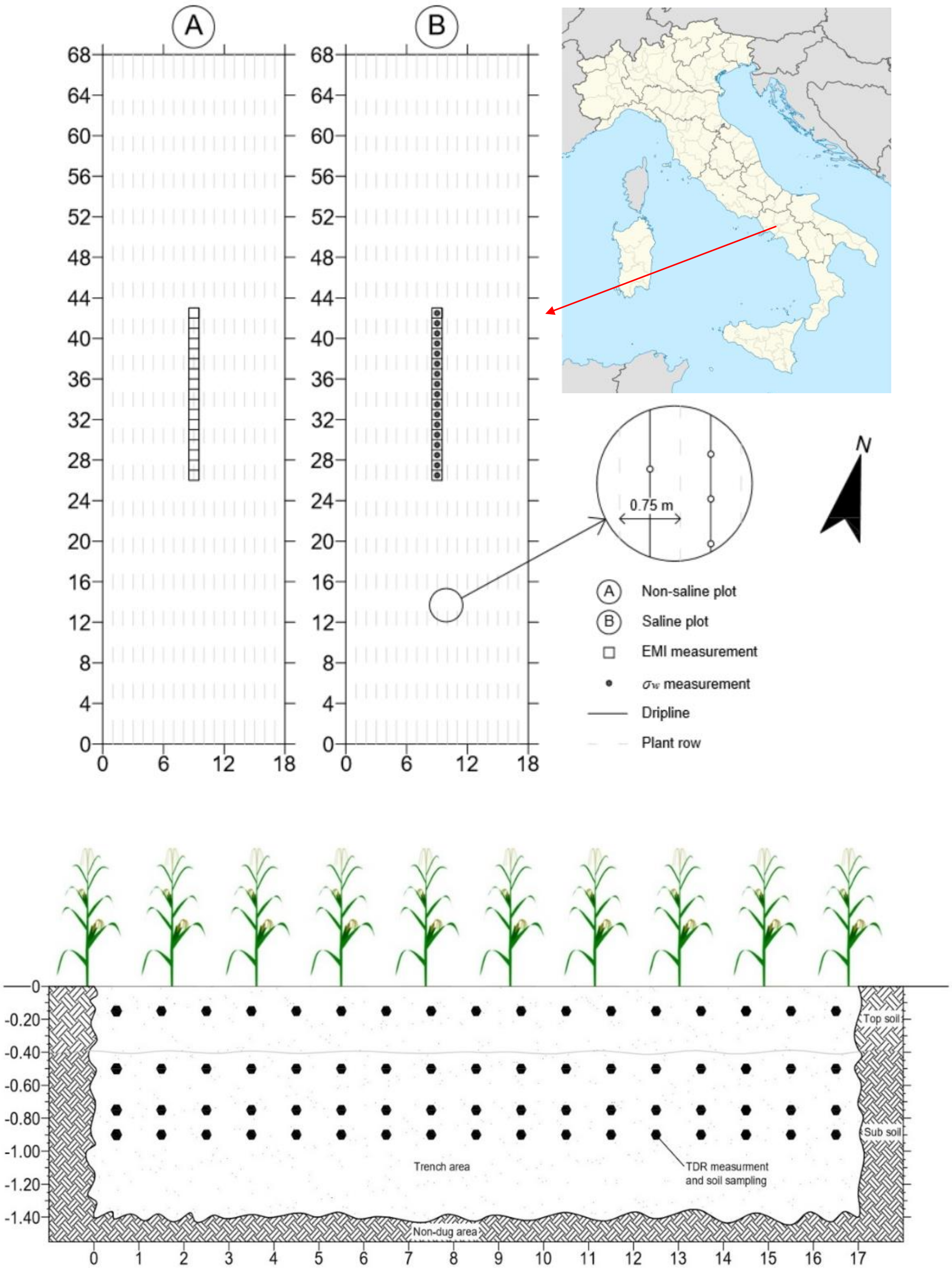

Figure 1: Schematic view of the experimental field (top panel) and front view of the trench showing measurement points (bottom panel). Map of Italy source: https://en.wikipedia.org/wiki/Platania#/media/File:Italy_provincial_location_map_2016.svg, last access 24/06/2025,

https://doi.org/10.5194/egusphere-2025-2696
Preprint. Discussion started: 25 June 2025

licensed under CC BY-SA.

2.2 Laboratory analysis

2.2.1 Soil-specific θ(ε) relationship.

The poorly crystalline clay minerals present at the experimental site significantly affect soil dielectric response (Bartoli et al., 2007; Regalado et al., 2003). Consequently, although Topp's (1980) θ(ε) relationship is generally applicable to most mineral soils, site-specific polynomial relationships were developed for the topsoil and subsoil to ensure accurate soil water content estimation.

Two PVC cylinders, each with a diameter of 8 cm and a height of 15 cm, were almost filled with air-dried soil to achieve a bulk density of approximately 1.1 g cm^{-3}, similar to that of undisturbed soil. The soil samples were then slowly saturated from the bottom, and a 12 cm long TDR probe was inserted from the top. During the evaporation process, both the sample weight and the dielectric permittivity were measured simultaneously. After 18 measurements, when changes in weight and ε were minimal, the soil samples were oven-dried at 105 °C for 24 hours to determine the volumetric water content. Finally, the θ–$\varepsilon^{0.5}$ pairs were fitted to a linear relationship.

2.2.2 Soil-specific θ(σ_b) relationship.

For each soil layer, five soil samples were collected using PVC cylinders (8 cm in diameter and 15 cm in height) from the non-saline plot. Each sample was wetted with 15 ml of $CaCl_2$ solution at specified electrical conductivities: 1, 3, 6, and 9 dS m^{-1}. This procedure was repeated about 20 times for each soil sample to cover a wide range of soil water content values, from air-dry (θ≈0.06 cm^3 cm^{-3}) to near saturation (θ≈0.46 cm^3 cm^{-3}) with increases in water content of approximately 0.02 cm^3 cm^{-3} for each application. For each sample, the procedure was stopped when the application volume led to visible drainage of the soil solution from the bottom of the cylinder.

For each wetting step, TDR three-wire probes (10 cm long with a rod diameter of 0.3 cm and rod spacing of 1.2 cm) were vertically inserted into the soil columns. Measurements of volumetric water content (θ) were taken using the topsoil-specific θ(ε) relationships, and bulk electrical conductivity (σ_b) was also measured, based on the TDR impedance, Z, obtained at large signal travel times (e.g., Robinson et al. 2003). The soil columns were covered with 0.05 mm plastic foil overnight to prevent evaporation and allowed to equilibrate at room temperature (20°C).

Finally, for each soil layer, a linear relationship between θ and σ_b was established by fitting the data pairs obtained.

2.2.3 Calibration of the Rhoades θ - σ_b - σ_w model.

Rhoades et al. (1976) proposed a linear model between σ_b and σ_w for a given θ value:

https://doi.org/10.5194/egusphere-2025-2696
Preprint. Discussion started: 25 June 2025

$$\sigma_b = \theta T \sigma_w + \sigma_s \quad (1)$$

in which T is the transmission coefficient, also known as tortuosity, which considers the tortuous nature of the current line and any decrease in the mobility of the solid-liquid and liquid-gas interfaces, whereas σ_s represents the electrical conductivity of the solid phase of the soil that is associated to the exchangeable ions in the solid-liquid interface.

Tortuosity linearly depends on θ and is characterised as follows:

$$T = a\,\theta + b \quad (2)$$

where a and b are parameters specific for each soil type estimated as a fitting parameter in eq. 1. σ_s is calculated using a graphical approach (Rhoades et al., 1976).

In order to calibrate the model for deriving the soil-specific a, b and σ_s parameters, the procedure reported in Malicki and Walczak (1999) was applied, by using the same experiment reported therein at the point 2.2.2. Finally, the obtained θ - σ_b - σ_w data were fitted to the Rhoades model to finalize the calibration procedure.

2.2.4 Soil solution electrical conductivity determination.

The soil solution electrical conductivity was determined on 1:2 volume extract method (Rhoades et al., 1999). In particular, the 68 air-dried soil samples collected from the trench were preliminary sieved through a 2 mm mesh to remove coarse fragments and roots. Subsequently, for each sample, a 1:2 soil-to-water suspensions were prepared using 50g of soil and 100ml of distilled water. Once the soil and water were combined, the suspension was stirred thoroughly to ensure the full dissolution of the soluble salt into the water. After mixing, the suspension was centrifuged to separate the solid particles from the liquid phase, allowing extract the soil solution. Finally, the electrical conductivity of the extracted soil solutions was measured using a calibrated EC meter (Alves et al., 2022). Subsequently, chloride concentration in the extracts was determined via titration (Mohr's Method). A linear regression model was then established between the measured electrical conductivity ($\sigma_{w\text{-}SS}$) and the corresponding chloride concentration, resulting in an empirical relationship of the form:

$$\sigma = 0.0028\,[Cl^-] + 0.068 \quad (3)$$

where σ is the electrical conductivity of extract (dS m^{-1}), $[Cl^-]$ is the chloride concentration (mg L^{-1}).

To estimate the electrical conductivity representative of field conditions, the chloride concentration was scaled to the measure soil water content (SWC) of each sample. The scaled chloride concentration was calculated as the ratio between the total chloride mass and the water mass in the soil sample. Finally, the scaled $[Cl^-]$ was used in eq. (3) to estimate the electrical conductivity, representative of the soil solution under its field water content conditions ($\sigma_{w\text{-}SS}$).

2.3 EMI and TDR analysis

The vertical distribution of bulk electrical conductivity ($\sigma_b(z)$) was obtained by inverting the EC_a dataset using EM4SOIL software (ENTOMO, 2018) by applying a 1-D laterally constrained method developed by Monteiro Santos (2004). The inversion algorithm employs a set of 1D conductivity models constrained by their neighbours, with forward

https://doi.org/10.5194/egusphere-2025-2696
Preprint. Discussion started: 25 June 2025

modelling based on the full solution of Maxwell's equations (Kaufman and Keller, 1983). All models used in the inversion have the same number of layers, and the thickness of these layers is kept constant.

Occam regularization (deGroot-Hedlin and Constable, 1990) and the S2 inversion algorithm (Sasaki, 2001) were utilized in this study. Occam regularization helps to stabilize the inversion process by constraining model variations around a reference model, making the results less sensitive to noisy data. The balance between data fit and neighbour constraints during inversion is controlled by an empirical multiplier (or damping factor). During the inversion process, damping factors, λ, decrease gradually to resolve more detailed parameters (e.g., Farzamian et al., 2019). Inversion results will generally be smoother if the values are larger. The best inversion parameters are usually achieved empirically after testing various parameter sets. In this study, the maximum number of iterations was set to 10, and the damping factor was set to 0.5.

The TDR technique, utilized for both field and laboratory measurements, allows for the estimation of θ and σ_b.

Soil water content is estimated by determining the soil permittivity using the Tektronix 1502 C, which measures the propagation time of electromagnetic waves generated by the pulse generator and detected by a sampling oscilloscope (Noborio, 2001). Permittivity (ε) is calculated based on the propagation velocity (v) of the electromagnetic waves, as described by:

$$\varepsilon = \left(\frac{c}{v}\right)^2 = \left(\frac{c \cdot t}{2\,L}\right)^2 \tag{4}$$

where c is the velocity of electromagnetic waves in a vacuum (3×10^8 m s^{-1}), t is the round-trip time for the pulse to traverse the length of the probe (down and back: 2L) [s], L is the TDR probe length [m].

The measurement of σ_b is based on the attenuation of the voltage pulse magnitude (Dalton et al., 1984). The Tektronix 1502 C measures the total resistance, R_T, of the transmission line using:

$$R_T = R_s + R_c = Z_c \frac{(1+\rho)}{(1-\rho)} \tag{5}$$

where: Rc is the series resistance from the cable and connector [Ω], Rs is the soil contribution to the total resistance [Ω], Zc is the characteristic impedance of the transmission line (50 Ω in this case), ρ is the voltage reflection coefficient at a large travel time, when the signal reflected at the end of the probe reaches a constant value (Comegna et al., 2017).

The σ_b at 25°C can be calculated as (Rhoades and Van Schilfgaarde, 1976) $\sigma_b = K_C/R_S \times f_T$, where K_c is the geometric (cell) constant of the TDR probe and f_T is a temperature correction factor to be used for values measured at temperatures other than 25°C. Both R_S and K_C can be determined in the laboratory by measuring R_T by TDR in a solution with known salinity.

2.4 A synthesis of the applied procedure

The flowchart of the proposed procedure is displayed in Fig. 2 and summarized in the following six steps:

https://doi.org/10.5194/egusphere-2025-2696
Preprint. Discussion started: 25 June 2025

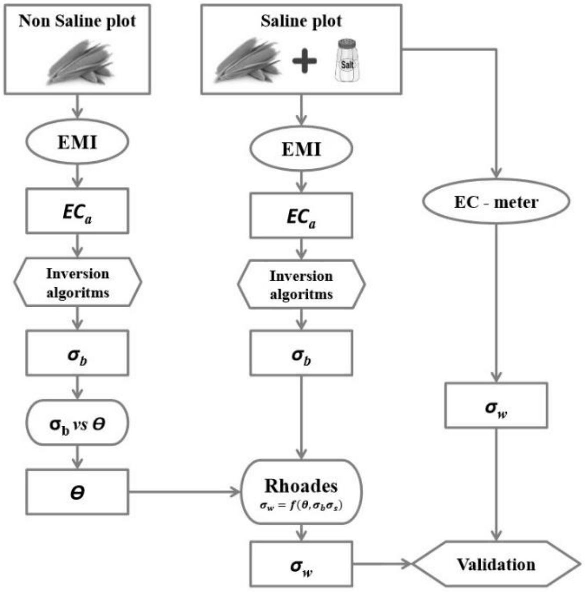

Figure 2: Flowchart of the proposed procedure.

1. **Irrigation and EMI Measurements:** Two plots, were irrigated with saline and plain water, respectively. EMI measurements were performed in both plots in order to obtain the distribution of the EC_a within the two plots.
2. **Inversion to obtain σ_b:** The σ_b distribution in both plots was calculated using an inversion procedure (see sections 3.1. and 3.3).
3. **Laboratory determination of $\theta(\sigma_b)$ relationship:** A soil-specific linear relationship $\theta - \sigma_b$ was determined in laboratory on soil not salinized.
4. **Determination of θ distribution in non-saline plot:** The distribution of soil water content in the non-saline plot was determined from the σ_b distribution (step 2) by using the relationship determined in step 3.
5. **Estimation of σ_w in the saline plot:** The spatial distribution of σ_w in the saline plot was estimated using the Rhoades et al. (1976) model incorporating the inverted σ_b values measured on saline plot and the average soil water content determined in the step 4. This estimation was based on the assumption that the mean and the variance of the soil water content distribution were similar in both plots.
6. **Validation of σ_w and θ**. The σ_w values estimated using the described procedure were validated by comparison to an independent σ_w dataset obtained in the laboratory through soil solution electrical conductivity (EC) measurements on bulk soil samples ($\sigma_{w\text{-}SS}$).

https://doi.org/10.5194/egusphere-2025-2696
Preprint. Discussion started: 25 June 2025

The reliability of the estimates was analysed based on root mean square values (Root Mean Square Error, RMSE) and the mean deviation (Bias), according to the following formulas:

$$\mathrm{RMSE} = \sqrt[2]{\frac{\sum_{i=1}^{n}\left(X_{m,i} - X_{es,i}\right)^2}{N}} \tag{6}$$

$$\mathrm{Bias} = \frac{\sum\left(X_{es,i} - X_{m,i}\right)}{N} \tag{7}$$

where X_m are the measured values, X_{es} are the estimated values at the time i and N is the number of measured values.

https://doi.org/10.5194/egusphere-2025-2696
Preprint. Discussion started: 25 June 2025

3 Results and Discussion

3.1 Laboratory experiments

3.1.1 Soil-specific θ(ε) relationship

Table 1 presents the coefficients α and β for the linear soil-specific relationship $\theta=\alpha+\beta\sqrt{\varepsilon}$, along with the coefficient of determination (R^2) for both topsoil (Ap horizon) and subsoil (Bw horizon), obtained from laboratory experiments. The equations for the Ap horizon and Bw horizon show similar intercepts but slightly different slopes, leading to a divergence between the two curves at higher soil water contents.

Table 1: Coefficients and R^2 values for the $\theta-\sqrt{\varepsilon}$, $\theta-\sigma_b$, and $\theta-\sigma_b-\sigma_w$ soil-specific calibration relationships

Horizon	Depth (cm)	Texture	Relationship (i) $\theta=\alpha+\beta\sqrt{\varepsilon}$			Relationship (ii) $\theta=a+b\,\sigma_b$			Rhoades model (iii) $\sigma_w=\frac{\sigma_b-\sigma_s}{\theta\,T}$			
			α	β	R^2	a	b	R^2	a	b	σ_s*	R^2
Ap	0-40	Loam	-0.133	0.113	0.96	0.189	0.575	0.83	1.32	-0.14	0.13	0.95
Bw	40-110	Sandy loam	-0.130	0.119	0.94	0.185	0.639	0.92	1.28	-0.12	0.07	0.97

* (dS m^{-1})

Figure 3 compares the two observed relationships with the linear form of Topp's equation. The findings indicate that Topp's equation consistently overestimates the water content, with an average overestimation of approximately 0.07 ± 0.01 $cm^3\ cm^{-3}$ in the Ap horizon and about 0.05 ± 0.02 $cm^3\ cm^{-3}$ in the Bw horizon. These discrepancies suggest that the application of Topp's equation may require local calibration to account for horizon-specific characteristics.

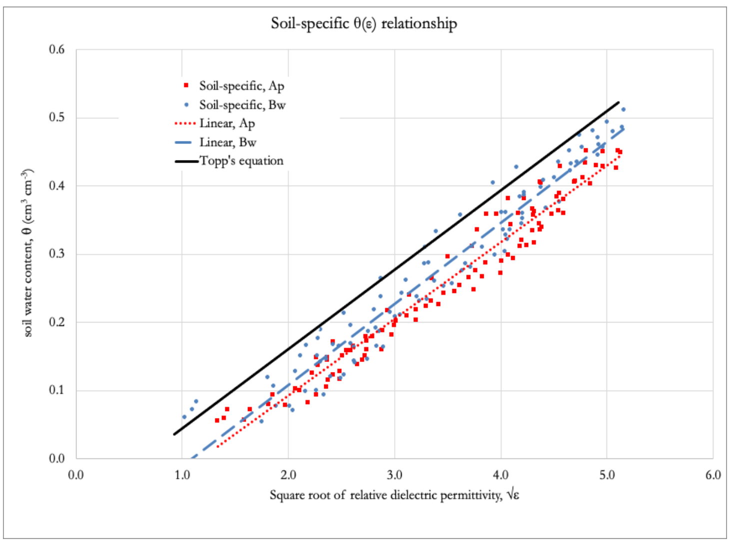

Figure 3: Soil specific linear relationship between the square root of relative dielectric permittivity and volumetric soil water content for the Ap and Bw horizons.

https://doi.org/10.5194/egusphere-2025-2696
Preprint. Discussion started: 25 June 2025

3.1.2 Soil-specific θ(σb) relationship [STEP 3]

Figure 4 compare the soil-specific linear relationship $\theta = a + b\ \sigma_b$, which enables the estimation of soil water content from bulk soil electrical conductivity measurements. for the Ap and Bw horizons. Table 1 shows the corresponding coefficients of the relationship, along with the coefficients of determination (R^2). The comparison highlights that while the intercept and slope values do not significantly differ between the two horizons, the R^2 values suggest a stronger correlation in the Bw horizon compared to the Ap horizon.

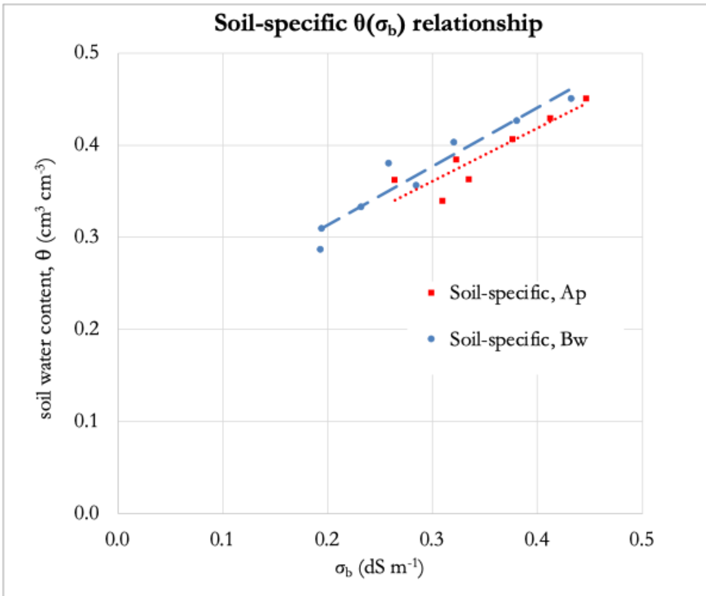

Figure 4: Soil specific linear relationship between the σ_b and volumetric soil water content for the Ap and Bw horizons.

3.1.3 Calibration of the Rhoades θ – σb – σw model [STEP 6]

Figure 5 presents the results of the laboratory experiment conducted using TDR to calibrate the parameters of the Rhoades et al. (1976) model (also reported in Table 1). For each soil water content, ranging from 0.15 to 0.40 $cm^3\ cm^{-3}$, σ_b increases linearly with σ_w within a range of 1 to 9 $dS\ m^{-1}$. The σ_s values at different soil water content levels converge towards 0.13 $dS\ m^{-1}$ for topsoil and 0.07 $dS\ m^{-1}$ for subsoil.

It's important to note that this relationship does not apply under dry soil conditions. In fact, the graphs show that as the water content decreases, the slope of the fitting line progressively flattens, becoming nearly horizontal at $\theta = 0.15\ cm^3\ cm^{-3}$. This suggests that σ_b becomes almost insensitive to changes in σ_w as the soil dries (Nadler, 1982; Rhoades et al., 1989).

https://doi.org/10.5194/egusphere-2025-2696
Preprint. Discussion started: 25 June 2025

According to Nadler (2005), the relationship at low θ values becomes impractical due to the complex interdependencies between various solid- and liquid-phase parameters that dominate as water content decreases.

This finding is crucial for this study's focus on using EMI for salinity and water content assessment, as it indicates that EMI measurements should be conducted in wet or moderately wet soils rather than dry soils. Moreover, it highlights that a reasonable soil moisture threshold for reliable measurements in the studied soil is greater than 0.15 cm^3 cm^{-3}.

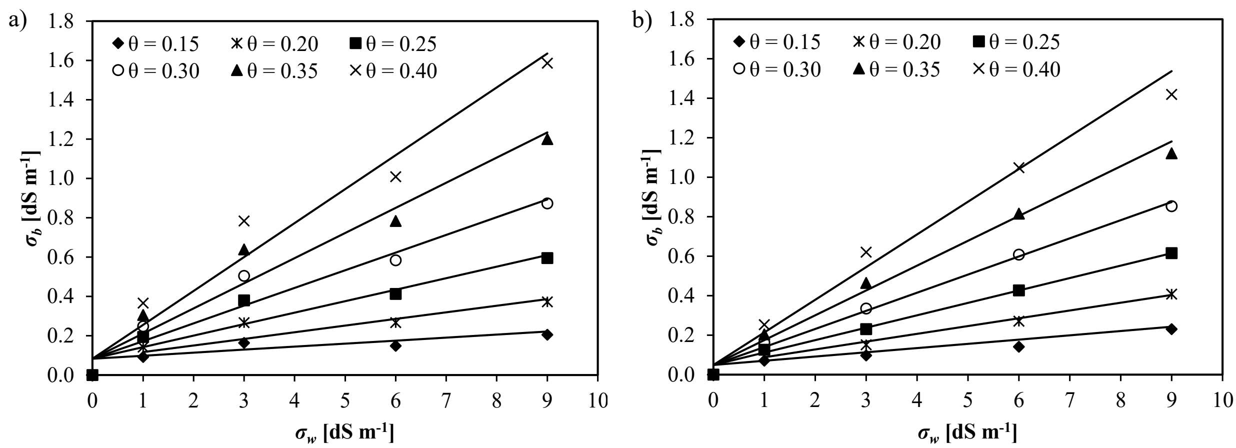

Figure 5: Bulk electrical conductivity (σ_b) measured by TDR vs. pore water electrical conductivity (σ_w) measured by an EC meter for six levels of soil water content (cm³ cm⁻³). The continuous lines represent the fitted Rhoades model (Eqs. 1 and 2) for (a) topsoil and (b) subsoil.

3.2 Estimation of θ by EMI measurements in the non-saline plot [STEP 2 – 4]

Figure 6 reports the spatial distribution of the measured apparent soil electrical conductivity (EC$_a$) under VCP configuration a) and HCP configuration b) for the three receiver coils ρ32, ρ71, and ρ118. The EC$_a$ values are generally low, ranging from 0.02 to 0.08 dS m^{-1}. The EC$_a$ data exhibit a similar pattern in both VCP and HCP modes, with slightly higher EC$_a$ values at ρ118 (1.2 m depth), intermediate values at ρ71 (0.7 m depth), and lower values at ρ32 (0.3 m depth). This trend suggests a more conductive zone at deeper layers. In terms of horizontal variability, the EC$_a$ in vertical mode shows relatively small variation, with coefficients of variation of 15%, 14%, and 13% for ρ118, ρ71, and ρ32, respectively. Even lower are the coefficients of variation in horizontal mode. Looking at the transect in Fig. 6a, an anomalous behaviour is revealed between 4.8 and 6.4 m. This anomaly is attributed to an old buried channel crossing the plot, which was uncovered during the excavation of the trench (see section 2.1). Although the soil within the channel, formed over more than 80 years, had undergone pedogenesis and appeared similar to the surrounding soil, the channel's contours remain distinct and recognizable.

https://doi.org/10.5194/egusphere-2025-2696
Preprint. Discussion started: 25 June 2025

Figure 6c presents the modelling results with estimation of σ_b distribution with depth along the profile. The misfit error is 0.01 mS m^{-1}, indicating a fairly good fit between the observed data and model responses. In terms of vertical variability, the σ_b values follow the trend of the observed data, showing a general increase with depth. This pattern suggests the presence of at least three distinct electrical layers, each with unique electrical and electromagnetic properties:

In the surface layer (0–30 cm), electrical conductivity exhibits medium-to-high values (0.03–0.08 dS m^{-1}), likely due to a combination of factors. These include low soil water content during the EMI measurement and a slight increase in salt concentration in the pore water caused by evaporation from the soil surface, which is wetted by surface drip irrigation. Furthermore, as reported by Bonfante et al. (2019), who studied the same soil, the upper layer has a higher clay content (10.5%) compared to the underlying layers. Given the well-established strong correlation between EC_a and clay content (Sudduth et al., 2005), it is reasonable to hypothesize that the clay content could influence the observed EC_a patterns in this surface layer.

The central layer (30–80 cm), characterized by a minimum in σ_b values forming a gradient that decreases from the top to the bottom of this layer. This zone is directly wetted by drip irrigation, coinciding with peak root activity and a decrease in clay content from 5.9% to 3.9% (Bonfante et al., 2019). Moreover, this layer is likely affected by downward leaching of salts and fertilizers into deeper layers through drip irrigation water (Corwin et al., 2022).

The third and deepest layer (below 90 cm) is characterized by a progressive increase in bulk electrical conductivity. This can be explained by the highest clay content in soil profile (11.6%), accumulation of soluble salts leached from the upper layers, combined with an increase in soil compaction with depth that reduces water storage capacity, related to the reduction of porosity in this zone.

Regarding lateral variability, the overall variability remains low across all depths, except for the zone corresponding to the old channel, which is clearly distinguishable. The presence of this channel likely contributes to localized differences in soil properties, (such as the bulk density), creating distinct pattern in the electrical conductivity profile.

https://doi.org/10.5194/egusphere-2025-2696
Preprint. Discussion started: 25 June 2025

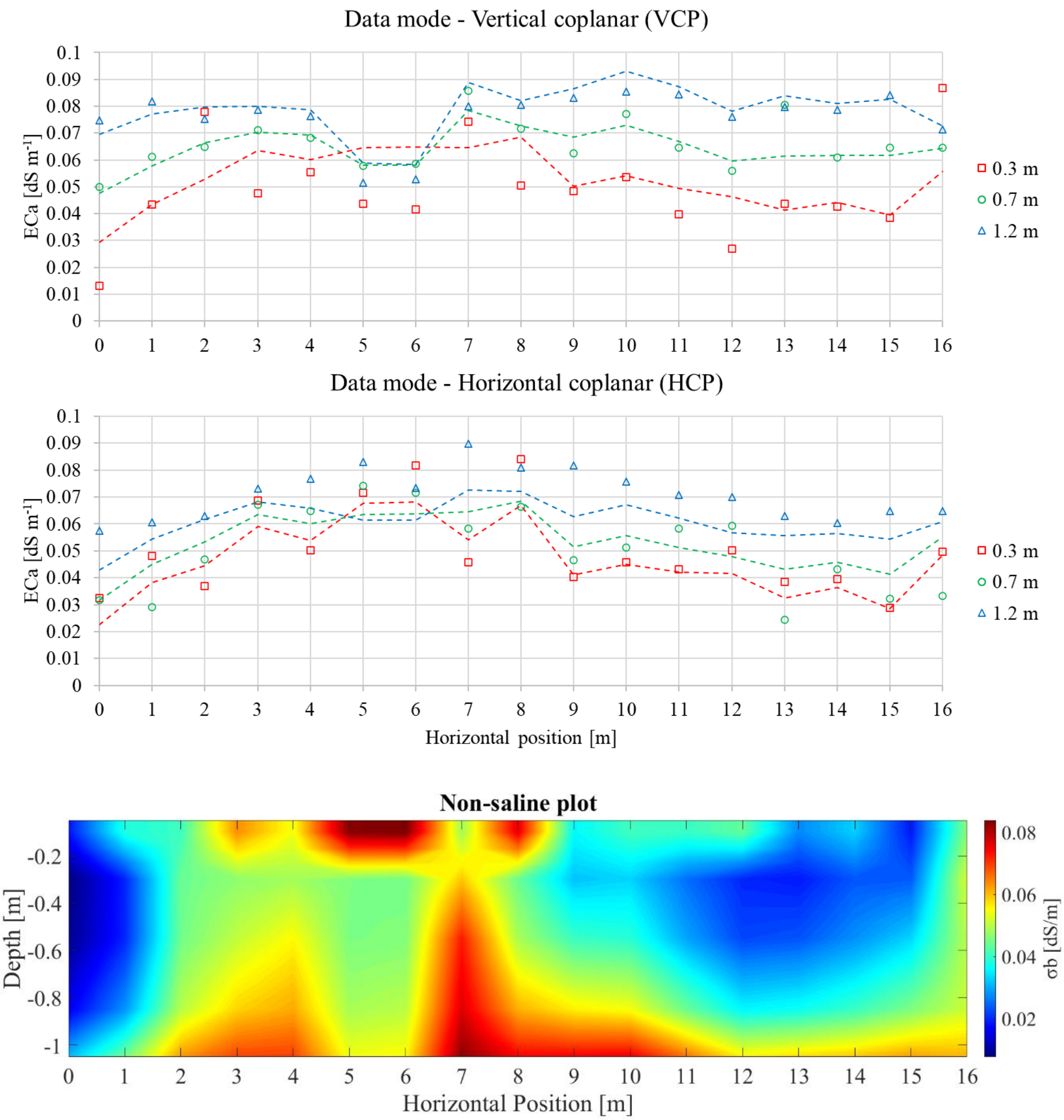

Figure 6: Spatial distribution of the measured apparent soil electrical conductivity (EC_a) (a) and the inversion modelling results with estimation of Bulk electrical conductivity (σ_b) distribution with depth (b) for the non-saline plot.

Figure 7 presents the θ values at four distinct depths (15, 50, 75, and 90 cm), derived from the soil-specific $\theta(\sigma_b)$ relationships detailed in Table 1 and correspond to the depths extracted from the image shown in Fig. 6c. Specifically, the

https://doi.org/10.5194/egusphere-2025-2696
Preprint. Discussion started: 25 June 2025

relationship for the Ap horizon was applied to the 15 cm depth, while the relationship for the Bw horizon was used for the deeper depths, aligning with the depths used for θ, σ_b, and σ_w measurements, as discussed in Section 3.4.

At depths of 50, 75, and 90 cm, the θ data series nearly overlap, with average soil water content values along each transect ranging between 0.20 cm^3 cm^{-3} (for 50 and 75 cm) and 0.21 cm^3 cm^{-3} (for 90 cm). The variability at these depths is minimal, with an average coefficient of variation of 3.4%. In contrast, the upper horizon (15 cm) shows a higher average soil water content of 0.23 cm^3 cm^{-3} and greater variability, with a coefficient of variation of 5.0. This suggests that deeper soil layers maintain more stable moisture conditions, while the upper horizon is more influenced by processes at boundary such as evaporation and infiltration.

Across all depths, higher values of soil water content are observed in the central part of the transect (7-12 m). This pattern corresponds to the higher σ_b values shown in the data presented in Fig. 6c, indicating an increase in soil water content in this section of the plot across the different depths.

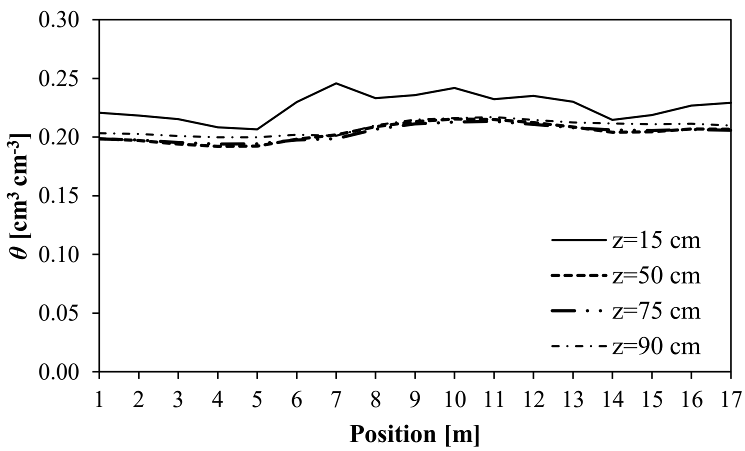

Figure 7: Spatial distribution of soil water content (θ) in the non-saline plot at four depths (15, 50, 75, and 90 cm), estimated from bulk electrical conductivity (σ_b) distribution.

3.3 Estimation of σ_w in the saline plot [STEP 2 – 5]

Figure 8a shows the EC_a measurements in both VCP and HCP modes for the three receiver coils ρ32, ρ71, and ρ118. The EC_a values are higher than those observed in the non-saline plot, ranging from 0.2 to 0.45 dS m^{-1}. Both VCP and HCP data display a similar pattern, with EC_a values decreasing from the upper layer (0.30 m) to the deeper layer (1.2 m), suggesting a more conductive topsoil, which is expected due to saline water irrigation. The differences are more pronounced in the VCP mode compared to the HCP mode. In terms of lateral variability, the EC_a in vertical mode exhibits relatively minor variation, with coefficients of variation of 15%, 14%, and 13% for ρ118, ρ71, and ρ32, respectively. Additionally,

https://doi.org/10.5194/egusphere-2025-2696
Preprint. Discussion started: 25 June 2025

higher EC_a values are observed in the central part of the plot, gradually decreasing towards the edges. Despite the presence of the old buried channel crossing the plot, no noticeable differences in EC_a are evident along this transect. This can be attributed to the dominant impact of soil salinity which masks the channel impact. The contribution of the channel is relatively minor (around 0.02 dS m^{-1}), as previously observed in Fig. 6a.

Figure 8c shows the σ_b distribution obtained from the inversion procedure of the EMI measurements conducted on 2nd August in the saline plot. As expected, the values of σ_b obtained from the inversion modelling were consistently higher in the saline plot compared to the non-saline plot. These values decreased from the surface to a depth of two metres, ranging from 0.55 to 0.10 dS m^{-1}. This pattern of declining σ_b with depth has also been reported by other authors (e.g., Saeed et al., 2017). During the irrigation season, salt accumulation tends to be concentrated in the topsoil layer (Coppola et al., 2015, 2016), largely due to evaporation at the soil surface, which causes salts to rise and concentrate in the upper layers (Corwin and Lesch, 2005; Kara and Willardson, 2006).

https://doi.org/10.5194/egusphere-2025-2696
Preprint. Discussion started: 25 June 2025

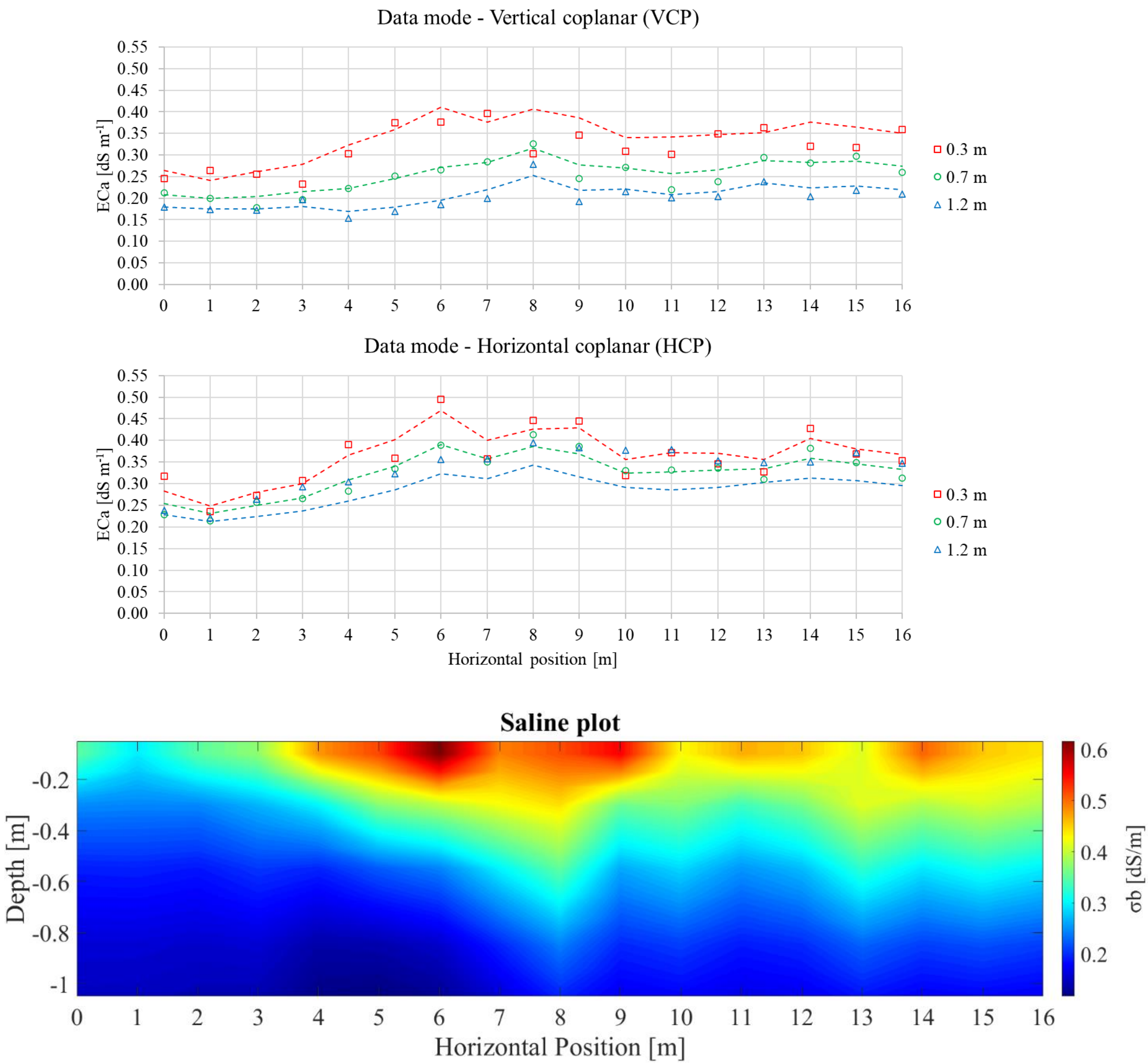

Figure 8: Spatial distribution of the measured apparent soil electrical conductivity (EC_a) under VCP configuration a) HCP configuration b), and the inversion modelling results with estimation of σ_b distribution with depth c) for the saline plot.

The Rhoades model was applied to estimate the electrical conductivity of the soil solution based on the σ_b measurements obtained from the EMI for both horizons. The laboratory calibrations provided the parameters *a*, *b*, and σ_s (as shown in Table 1), while θ was assumed as the average value measured in the non-saline plot (an average value for each of

340 the four depths, as seen in Fig. 7). In addition, to account for the variability of water content in the non-saline plot—and consequently, the error associated with its estimation, which influences the σ_w estimation procedure—the analysis was also conducted by using the mean water content value plus or minus its standard deviation. In this way, the validity of using the average value of the non-saline plot was numerically tested and further supported by additional considerations discussed in Section 3.5.

345 **3.4 Validation of σ_w estimated by EMI [STEP 6]**

Validation of the $\sigma_{w,EMI}$ estimation was carried out by comparing it with soil solution electrical conductivities measurements, $\sigma_{w,SS}$. Fig. 10 illustrates the results for four depths: 15 cm, 50 cm, 75 cm, and 90 cm. In the figures, the data series for $\sigma_{w,EMI}$ are represented by continuous lines, while $\sigma_{w,SS}$ values are shown as filled squares. To account for small-scale heterogeneity in $\sigma_{w,SS}$ – arising from the differing observation scales of the two data series –a simple moving average
350 filter was applied to smooth the $\sigma_{w,SS}$ data. As a result, the influence of individual measurements (short-term fluctuations) was minimized, while preserving the overall trend along the transect (long-term fluctuations) (Dragonetti et al., 2018; Western and Blöschl, 1999).

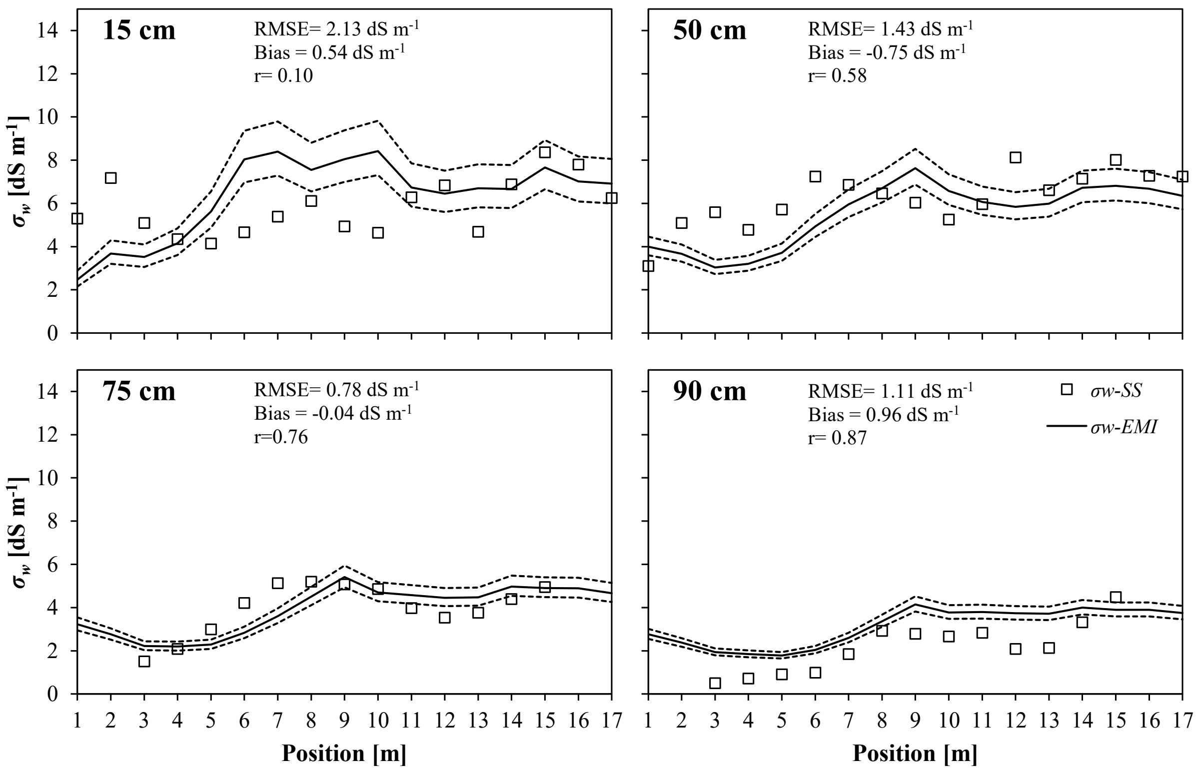

355 **Figure 9: Spatial distribution of σ_w within the trench at four depths (15, 50, 75 and 90 cm). The continuous lines represent $\sigma_{w,EMI}$, while the filled squares indicate the measured $\sigma_{w,SS}$ after applying a filtering process. The dotted lines denote the variability range of $\sigma_{w,EMI}$, computed based of one standard deviation of θ as measured in the non-saline plot.**

https://doi.org/10.5194/egusphere-2025-2696
Preprint. Discussion started: 25 June 2025

The largest discrepancies between measured and estimated σ_w values occur at a depth of 15 cm, with significant scatter around the mean (RMSE = 2.13 dS m^{-1}) and a relatively high overestimation (bias = 0.54 dS m^{-1}). At the other three depths, the data show better agreement, with RMSE values below 1.43 dS m^{-1} and bias ranging from -0.75 to 0.96 dS m^{-1}.

As depth increases, the correlation coefficient between the two series rises from 0.23 in the upper layer to 0.87 in the deeper layer. The graphs in Fig. 9 also show the $\sigma_{w,EMI}$ estimates obtained by assuming, at each depth considered, the average plus/minus the standard deviation of the water contents measured under the non-saline transect (dotted lines). Note that the uncertainty in the $\sigma_{w,EMI}$ estimations coming from the assumption of similarity between the two plots in terms of water contents is quite high only for the data at 15 cm. assuming the average content and decreases drastically with depth, maybe as an effect of the variability in soil water content. This issue is discussed in detail later in a dedicated section.

As suggested by Robinet et al. (2018) who analysed the reasons behind discrepancies in σ_b detected by sensors operating at different observation volumes – similar to our case – the weak correlation between EMI and soil sampling measurements for a shallow sensing coil configuration and the forward-calculated EC_a can be attributed to several factors. Firstly, significant variations in σ_b near the soil surface may not be effectively captured by local soil sampling. Secondly, the uneven and irregular nature of the soil surface can significantly impact EMI measurements. Variations in elevation and rough terrain make it difficult for the operator to keep the instrument at a constant height above the ground. Since EMI measurements are highly sensitive to the distance between the sensor and the soil, any fluctuations in height can introduce inconsistencies in the data, potentially affecting the accuracy and reliability of the results. Thirdly, σ_b measurements are influenced by the maize root system, which is denser in the shallower soil layer, further impacting the readings. These factors contribute to the relatively high variance observed at 15 cm in EMI measurements ($\sigma_{w,EMI}$), which decreases with depth (see Table 2). By contrast, the same table shows that the variance $\sigma_{w,SS}$ increases considerably with depth.

Table 2: Values of variance for the σ_w measurement by EMI, $\sigma_{w\text{-}EMI}$, soil solution, $\sigma_{w,SS}$ and filtered soil solution data $\sigma_w^{SS\text{-}f}$

Depth [cm]	**Variance** [dS^2 m^{-2}]	
	$\sigma_{w,EMI}$	$\sigma_{w,SS}$
15	3.38	1.60
50	2.12	1.64
75	1.21	1.41
90	0.75	1.36

3.5 Validation of θ estimated by EMI [STEP 6]

The procedure was further validated by comparing the soil water content estimated by EMI with an independent series of water content measurements taken by TDR in the saline plot immediately after the EMI readings. While this comparison was not strictly required for the procedure, it serves to corroborate the assumptions and findings discussed. In

https://doi.org/10.5194/egusphere-2025-2696
Preprint. Discussion started: 25 June 2025

fact, the concept of validation has a twofold meaning. On one hand, it allows us to assess whether the estimated values, obtained through the six-step procedure outlined in Fig. 1, align with the measured ones. On the other hand, it verifies whether the value estimated from the non-saline plot effectively corresponds to the one measured in the same plot. Additionally, validation provides insights into the variability of the estimate compared to the actual measurements.

Figure 10 presents the data series for soil water content estimated by EMI (θ_{EMI}), derived from EMI measurements following the outlined procedure, shown as continuous lines. Alongside these, the measured water content values from TDR (θ_{TDR}) are represented by filled squares. Each panel in Fig. 10 also includes statistical parameters – root mean square error (RMSE), bias, and correlation coefficient (r) – which assess the agreement between the θ_{EMI} and θ_{TDR} series.

The water content at each depth remains approximately constant throughout the transect, indicating notable homogeneity in the horizontal plane. This observation supports the fundamental hypothesis of the study. Across the four depths, the average values of θ_{EMI} ranged between 0.20 and 0.23 cm^3 cm^{-3}, with a mean error (RMSE) of 0.01 cm^3 cm^{-3} and a slight underestimation of -0.004 cm^3 cm^{-3}.

A weak correlation was observed in the topsoil, where the correlation coefficient between θ_{EMI} and θ_{TDR} was low, with values of r = 0.15 and 0.24 at depths of 15 cm and 50 cm, respectively. In contrast, a strong correlation was observed in the subsoil at depths of 75 cm and 90 cm, whit r values of 0.88 and 0.89, respectively. This trend of increasing correlation from topsoil to subsoil is consistent with previous studies, such as Calamita et al. (2015), which reported similar patterns.

https://doi.org/10.5194/egusphere-2025-2696
Preprint. Discussion started: 25 June 2025

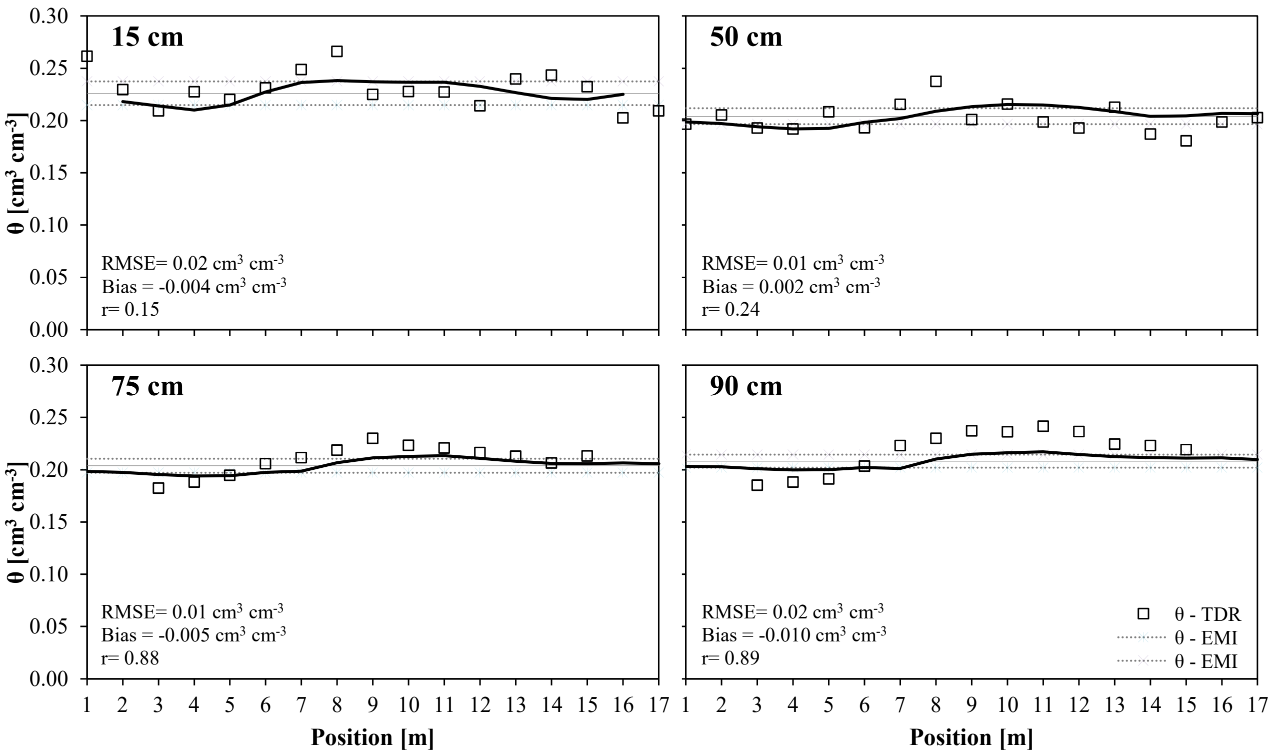

Figure 10: Spatial distribution of soil water content data within the trench for four depths (15, 50, 75 and 90 cm) as measured by TDR and estimated by EMI. The TDR data are represented by filled square, while the EMI data are represented by a continuous solid line. The dashed line represents the average water content as measured by EMI in the non-saline transect

In this section are shown the results of a sensitivity analysis was carried out to quantify the impact of using the average θ obtained at different depths in the non-saline transect when analysing data from the saline transect. The dotted lines in the four plots of Figure 10 represent the range of variability of $\sigma_{w,EMI}$, calculated based on the standard deviation of θ as measured in the non-saline plot. Regarding correlation and RMSE, the impact of soil water content variability on the σ_w estimate decreases with increasing measurement depth. At 15 cm, the effect is relatively pronounced, whereas at greater depths, it becomes negligible. This finding underscores the robustness of the obtained values, with minimal uncertainty at deeper layers. However, at 15 cm, the estimates are less reliable. In fact, various studies have highlighted the impact of θ variability on soil salinity estimation, particularly within the root zone, where significant fluctuations in θ occur due to irrigation practices and evaporation (e.g., Gómez Flores et al., 2022; Paz et al., 2020).

3.6 Limits and conditions of use of the procedure

The procedure assumes that the average soil water content in the saline plot is similar to that in the non-saline plot for each soil horizon. To support this assumption, in our case study:

1. A study by Bonfante et al. (2019) at the same site established the pedo-hydrological similarity between the two plots. Their Fig. 2 illustrates that the soils and horizons in both plots exhibit very similar hydrological and physical properties.
2. Throughout the growing season, both plots were managed identically:
   - They received the same irrigation volumes and followed the same irrigation schedule.
   - Maize was sown on the same day in both plots.
   - The first saline irrigation was applied on June 6th—approximately 50 days after sowing (April 16th)—to prevent early stress and minimize its impact on crop development.
   - Physiological measurements, including phenological phase and root depth, were comparable across both plots.
3. Water Uptake and Crop Response:
   - Leaf water potential measurements showed no significant differences throughout the irrigation. A t-test confirmed the absence of significant differences between the plots ($p > 0.05$), indicating similar water uptake conditions.

In summary, given the nearly identical soil and sequence of soil horizons, their corresponding hydraulic properties, and the identical irrigation regime, it is reasonable to assume that the mean water content in each horizon is similar in both plots. This assumption is further supported by the mostly overlapping water uptake and physiological status of maize during the irrigation season.

In a context of relative soil homogeneity and similar agricultural management, the procedure yielded satisfactory results. Therefore, the procedure's effectiveness diminishes when applied on a larger scale or to heterogeneous soil conditions.

However, if the experimental conditions revealed at our site are not available, the applicability of the method may be challenged. In such cases, adjustments would help ensure the reliability and robustness of the procedure in different environmental and agronomic contexts.

In principle, the procedure is specifically designed for soils experiencing secondary salinization due to irrigation, which facilitates the identification of similar non-saline soils on the same farm. Applying this procedure to soils with primary salinization presents is more challenging, due to the absence of such reference conditions. Nevertheless, this limitation is partially addressable. The average soil water content for each layer could be independently measured using alternative methods and applied directly to the saline plot, thereby eliminating the need for a reference non-saline plot. For instance, installing a network of soil moisture probes adequately calibrated and strategically placed across the field could provide the necessary data to apply the proposed methodology. In this case, the adequate placement of soil moisture sensors plays a crucial role in ensuring the representativeness and accuracy of the measurements. Variability field maps derived from EC_a measurements could be used preliminary to identify zones with homogeneous soil properties and the sensors could be

https://doi.org/10.5194/egusphere-2025-2696
Preprint. Discussion started: 25 June 2025

strategically positioned within these zones to capture a comprehensive profile of soil water content required to apply the proposed procedure extensively throughout the field. This solution could be broadening the potential applicability of the procedure to other contexts, eliminating the need for a non-saline plot and considering the soils spatial variability.

4 Conclusions

This study introduces a novel procedure for quickly distinguishing the contributions of water content and salinity in electromagnetic induction (EMI) measurements of apparent electrical conductivity (EC_a) providing a valuable tool for soil and water management. We conducted EC_a measurements along two adjacent parallel transects: one irrigated with non-saline water and the other with saline water. We utilized electrical conductivity levels of 1 dS m^{-1} (considered the non-saline level) and 8 dS m^{-1} for comparison.

The proposed procedure is based on the hypothesis that the average soil water content in the saline transect is "similar" to that in the adjacent non-saline transect. Given the similar soil physical properties, hydrology, irrigation distribution, and fertilization practices expected in both transects, we anticipate comparable agronomic conditions. This can lead to similar root distributions and nutrient uptake patterns, ultimately resulting in analogous water content distributions. Our findings support the validity of this hypothesis, as evidenced by the strong correlation between σ_w estimated via EMI and σ_w measured directly from soil solutions extracted from samples.

When the hypothesis holds, the proposed procedure is relatively straightforward to implement, addressing a key challenge in EMI application, distinguishing the effects of soil water content and salinity. To the best of our knowledge, this represents the first field-scale attempt to differentiate these effects in EMI measurements.

Despite the promising results, certain limitations must be acknowledged. Firstly, the underlying assumption of similar average soil water content limits the applicability of the proposed procedure, and, therefore, the procedure's effectiveness diminishes when applied on a larger scale or to heterogeneous soil conditions. Secondly, the procedure is specifically designed for soils experiencing secondary salinization due to irrigation, which facilitates the identification of similar non-saline soils on the same farm. Applying this procedure to soils with primary salinization presents is more challenging, due to the absence of such reference conditions.

Finally, the reliability of the EMI method tends to diminish at the soil surface, which can lead to less accurate results. however, with the fast development of EMI sensors equipped with a greater number of receivers and/or frequencies, the accuracy of EMI at soil surface may improve to some extent.

Future research should aim to validate the hypothesis of similar water content distribution in shallower soil layers, which often exhibit more erratic dynamics and less consistent results. To enhance this validation, the proposed procedure could be integrated with simulations of soil water flow using hydrological models, alongside appropriate top boundary conditions applied in the field experiment.

https://doi.org/10.5194/egusphere-2025-2696
Preprint. Discussion started: 25 June 2025

Competing interests:

The authors declare that they have no conflict of interest.

Financial support:

This research was performed within the project "SALTFREE: Salinization in irrigated areas: risk evaluation and prevention", funded by the MIPAAF (Ministry of Agriculture) under the call ARIMNET2.

https://doi.org/10.5194/egusphere-2025-2696
Preprint. Discussion started: 25 June 2025

References

Altdorff, D., Galagedara, L., Nadeem, M., Cheema, M., and Unc, A.: Effect of agronomic treatments on the accuracy of soil moisture mapping by electromagnetic induction, Catena (Amst), 164, 96–106, https://doi.org/10.1016/j.catena.2017.12.036, 2018.

Alves, A. C., de Souza, E. R., de Melo, H. F., Oliveira Pinto, J. G., de Andrade Rego Junior, F. E., de Souza Júnior, V. S., Adriano Marques, F., do Santos, M. A., Schaffer, B., and Raj Gheyi, H.: Comparison of solution extraction methods for estimating electrical conductivity in soils with contrasting mineralogical assemblages and textures, Catena (Amst), 218, 1–9, https://doi.org/https://doi.org/10.1016/j.catena.2022.106581, 2022.

Badewa, E., Unc, A., Cheema, M., Kavanagh, V., and Galagedara, L.: Soil moisture mapping using multi-frequency and multi-coil electromagnetic induction sensors on managed podzols, Agronomy, 8, https://doi.org/10.3390/agronomy8100224, 2018.

Bartoli, F., Regalado, C. M., Basile, A., Buurman, P., and Coppola, A.: Physical properties in European volcanic soils: a synthesis and recent developments, in: Soils of Volcanic Regions in Europe, edited by: Arnalds, Ó., Óskarsson, H., Bartoli, F., Buurman, P., Stoops, G., and García-Rodeja, E., Springer, Berlin, Heidelberg, 515–537, https://doi.org/https://doi.org/10.1007/978-3-540-48711-1_36, 2007.

Bonfante, A., Monaco, E., Manna, P., De Mascellis, R., Basile, A., Buonanno, M., Cantilena, G., Esposito, A., Tedeschi, A., De Michele, C., Belfiore, O., Catapano, I., Ludeno, G., Salinas, K., and Brook, A.: LCIS DSS—An irrigation supporting system for water use efficiency improvement in precision agriculture: A maize case study, Agric Syst, 176, 1–14, https://doi.org/10.1016/j.agsy.2019.102646, 2019.

Bouksila, F., Persson, M., Berndtsson, R., and Bahri, A.: Soil water content and salinity determination using different dielectric methods in saline gypsiferous soil, Hydrological Sciences Journal, 53, 253–265, https://doi.org/https://doi.org/10.1623/hysj.53.1.253, 2008.

Brevik, E. C., Fenton, T. E., and Lazari, A.: Soil electrical conductivity as a function of soil water content and implications for soil mapping, Precis Agric, 7, 393–404, https://doi.org/10.1007/s11119-006-9021-x, 2006.

Brouwer, C., Goffeau, A., and Heibloem, M.: Irrigation Water Management: Training Manual No. 1-Introduction to Irrigation., FAO Land and Water Development Division, Rome, Italy, 1985.

Calamita, G., Perrone, A., Brocca, L., Onorati, B., and Manfreda, S.: Field test of a multi-frequency electromagnetic induction sensor for soil moisture monitoring in southern Italy test sites, J Hydrol (Amst), 529, 316–329, https://doi.org/10.1016/j.jhydrol.2015.07.023, 2015.

Campbell, R. B., Bower, C. A., and Richards, L. A.: Change of Electrical Conductivity With Temperature and the Relation of Osmotic Pressure to Electrical Conductivity and Ion Concentration for Soil Extracts 1, Soil Science Society of America Journal, 66, 66–69, https://doi.org/https://doi.org/10.2136/sssaj1949.036159950013000C0010x, 1949.

https://doi.org/10.5194/egusphere-2025-2696
Preprint. Discussion started: 25 June 2025

Comegna, A., Coppola, A., Dragonetti, G., Severino, G., and Sommella, A.: Interpreting TDR Signal Propagation through Soils with Distinct Layers of Nonaqueous-Phase Liquid and Water Content, Vadose Zone Journal, 16, vzj2017.07.0141, https://doi.org/https://doi.org/10.2136/vzj2017.07.0141, 2017.

Coppola, A., Chaali, N., Dragonetti, G., Lamaddalena, N., and Comegna, A.: Root uptake under non-uniform root-zone salinity, Ecohydrology, 8, 1363–1379, https://doi.org/10.1002/eco.1594, 2015.

Coppola, A., Smettem, K., Ajeel, A., Saeed, A., Dragonetti, G., Comegna, A., Lamaddalena, N., and Vacca, A.: Calibration of an electromagnetic induction sensor with time-domain reflectometry data to monitor rootzone electrical conductivity under saline water irrigation, Eur J Soil Sci, 67, 737–748, https://doi.org/10.1111/ejss.12390, 2016.

Corwin, D. L. and Lesch, S. M.: Apparent soil electrical conductivity measurements in agriculture, Comput Electron Agric, 46, 11–43, https://doi.org/10.1016/j.compag.2004.10.005, 2005.

Corwin, D. L., Scudiero, E., and Zaccaria, D.: Modified ECa – ECe protocols for mapping soil salinity under micro-irrigation, Agric Water Manag, 269, 1–12, https://doi.org/10.1016/j.agwat.2022.107640, 2022.

Dalton, F. N., Herkelrath, W. N., Rawlins, D. S., and Rhoades, J. D.: Time-Domain Reflectometry: Simultaneous Measurement of Soil Water Content and Electrical Conductivity with a Single Probe, Science, New Series, 224, 989–990, 1984.

deGroot-Hedlin, C. and Constable, S.: Occam's inversion to generate smooth, two-dimensional models from magnetotelluric data, Geophysics, 55, 1613–1624, https://doi.org/https://doi.org/10.1190/1.1442813, 1990.

Doolittle, J. A. and Brevik, E. C.: The use of electromagnetic induction techniques in soils studies, Geoderma, 223–225, 33–45, https://doi.org/10.1016/j.geoderma.2014.01.027, 2014.

Dragonetti, G., Comegna, A., Ajeel, A., Piero Deidda, G., Lamaddalena, N., Rodriguez, G., Vignoli, G., and Coppola, A.: Calibrating electromagnetic induction conductivities with time-domain reflectometry measurements, Hydrol Earth Syst Sci, 22, 1509–1523, https://doi.org/10.5194/hess-22-1509-2018, 2018.

Dragonetti, G., Farzamian, M., Basile, A., Monteiro Santos, F., and Coppola, A.: In situ estimation of soil hydraulic and hydrodispersive properties by inversion of electromagnetic induction measurements and soil hydrological modeling, Hydrol Earth Syst Sci, 26, 5119–5136, https://doi.org/10.5194/hess-26-5119-2022, 2022.

ENTOMO: Manual for EM4Soil, 2018. A Program for 1-D Laterally Constrained Inversion of EM Data, 2018.

Farzamian, M., Paz, M. C., Paz, A. M., Castanheira, N. L., Gonçalves, M. C., Monteiro Santos, F. A., and Triantafilis, J.: Mapping soil salinity using electromagnetic conductivity imaging—A comparison of regional and location-specific calibrations, Land Degrad Dev, 30, 1393–1406, https://doi.org/10.1002/ldr.3317, 2019.

Farzamian, M., Autovino, D., Basile, A., De Mascellis, R., Dragonetti, G., Monteiro Santos, F., Binley, A., and Coppola, A.: Assessing the dynamics of soil salinity with time-lapse inversion of electromagnetic data guided by hydrological modelling, Hydrol Earth Syst Sci, 25, 1509–1527, https://doi.org/10.5194/hess-25-1509-2021, 2021.

Ghazouani, H., M'Hamdi, B. D., Autovino, D., Bel Haj, A. M., Rallo, G., Provenzano, G., and Boujelben, A.: Optimizing subsurface dripline installation depth with Hydrus 2D/3D to improve irrigation water use efficiency in the central Tunisia, International Journal of Metrology and Quality Engineering, 6, 1–8, https://doi.org/10.1051/ijmqe/2015024, 2015.

Gómez Flores, J. L., Ramos Rodríguez, M., González Jiménez, A., Farzamian, M., Herencia Galán, J. F., Salvatierra Bellido, B., Cermeño Sacristan, P., and Vanderlinden, K.: Depth-Specific Soil Electrical Conductivity and NDVI Elucidate Salinity Effects on Crop Development in Reclaimed Marsh Soils, Remote Sens (Basel), 14, 1–20, https://doi.org/10.3390/rs14143389, 2022.

Hilhorst, M. A.: A Pore Water Conductivity Sensor, Soil Science Society of America Journal, 64, 1922–1925, https://doi.org/https://doi.org/10.2136/sssaj2000.6461922x, 2000.

Huang, J., Scudiero, E., Bagtang, M., Corwin, D. L., and Triantafilis, J.: Monitoring scale-specific and temporal variation in electromagnetic conductivity images, Irrig Sci, 34, 187–200, https://doi.org/10.1007/s00271-016-0496-6, 2016.

IUSS Working Group WRB: World Reference Base for Soil Resources 2014, Update 2015. International Soil Classification System for Naming Soils and Creating Legends for Soil Maps. World Soil Resources Reports No. 106, FAO, Rome, https://doi.org/https://doi.org/10.1017/S0014479706394902, 2015.

Kara, T. and Willardson, L. S.: Leaching Requirements to Prevent Soil Salinization, 6, 1481–1489, https://doi.org/10.3923/jas.2006.1481.1489, 2006.

Kaufman, A. and Keller, G. V.: Frequency and Transient Sounding Methods in Geochemistry and Geophysics, Elsevier, Amsterdam, 686 pp., 1983.

Malicki, M. A. and Walczak, R. T.: Evaluating soil salinity status from bulk electrical conductivity and permittivity, Eur J Soil Sci, 50, 505–514, https://doi.org/https://doi.org/10.1046/j.1365-2389.1999.00245.x, 1999.

McNeill, J. D.: Electromagnetic Terrain Conductivity Measurement at Low Induction Numbers, Ontario, Canada, 1–15 pp., 1980.

Mester, A., van der Kruk, J., Zimmermann, E., and Vereecken, H.: Quantitative Two-Layer Conductivity Inversion of Multi-Configuration Electromagnetic Induction Measurements, Vadose Zone Journal, 10, 1319–1330, https://doi.org/10.2136/vzj2011.0035, 2011.

Monteiro Santos, F. A.: 1-D laterally constrained inversion of EM34 profiling data, J Appl Geophy, 56, 123–134, https://doi.org/10.1016/j.jappgeo.2004.04.005, 2004.

Mualem, Y. and Friedman, S. P.: Theoretical Prediction of Electrical Conductivity in Saturated and Unsaturated Soil, Water Resour Res, 27, 2771–2777, https://doi.org/10.1029/91WR01095, 1991.

Muñoz-Carpena, R., Regalado, C. M., Ritter, A., Alvarez-Benedí, J., and Socorro, A. R.: TDR estimation of electrical conductivity and saline solute concentration in a volcanic soil, Geoderma, 124, 399–413, https://doi.org/10.1016/j.geoderma.2004.06.002, 2005.

Nadler, A.: Estimating the Soil Water Dependence of the Electrical Conductivity Soil Solution/Electrical Conductivity Bulk Soil Ratio, Soil Science Society of America Journal, 46, 722–726, https://doi.org/https://doi.org/10.2136/sssaj1982.03615995004600040011x, 1982.

Nadler, A.: Methodologies and the practical aspects of the bulk soil EC (sa)-soil solution EC (sw) relations, Bet Dagan, Israel, 50250, 1–40 pp., 2005.

Nadler, A., Frenkel, H., and Mantell, A.: Applicability of the Four-Probe Technique under Extremely Variable Water Contents and Salinity Distribution1, Soil Science Society of America Journal, 48, 1258–1261, https://doi.org/https://doi.org/10.2136/sssaj1984.03615995004800060011x, 1984.

Noborio, K.: Measurement of soil water content and electrical conductivity by time domain reflectometry: a review, Comput Electron Agric, 31, 213–237, https://doi.org/https://doi.org/10.1016/S0168-1699(00)00184-8, 2001.

de Oliveira, A. B., Mendes Alencar, N. L., and Gomes-Filho, E.: Comparison Between the Water and Salt Stress Effects on Plant Growth and Development, in: Responses of Organisms to Water Stress, InTech, https://doi.org/10.5772/54223, 2013.

Paz, M. C., Farzamian, M., Paz, A. M., Castanheira, N. L., Gonçalves, M. C., and Santos, F. M.: Assessing soil salinity dynamics using time-lapse electromagnetic conductivity imaging, SOIL, 6, 499–511, https://doi.org/10.5194/soil-6-499-2020, 2020.

Rasool, S., Hameed, A., Azooz, M. M., Muneeb-U-Rehman, Siddiqi, T. O., and Ahmad, P.: Salt stress: Causes, types and responses of plants, in: Ecophysiology and Responses of Plants under Salt Stress, edited by: Ahmad, P., Azooz, M. M., and Prasad, M. N. V., Springer New York, New York, 1–24, https://doi.org/10.1007/978-1-4614-4747-4_1, 2013.

Regalado, C. M., Muñz Carpena, R., Socorro, A. R., and Hernández Moreno, J. M.: Time domain reflectometry models as a tool to understand the dielectric response of volcanic soils, Geoderma, 117, 313–330, https://doi.org/10.1016/S0016-7061(03)00131-9, 2003.

Rhoades, J. D. and Van Schilfgaarde, J.: An Electrical Conductivity Probe for Determining Soil Salinity, Soil Science Society of America Journal, 40, 647–651, https://doi.org/https://doi.org/10.2136/sssaj1976.03615995004000050016x, 1976.

Rhoades, J. D., Raats, P. A. C., and Prather, R. J.: Effects of Liquid-phase Electrical Conductivity, Water Content, and Surface Conductivity on Bulk Soil Electrical Conductivity 1, Soil Science Society of America Journal, 40, 651–655, https://doi.org/https://doi.org/10.2136/sssaj1976.03615995004000050017x, 1976.

Rhoades, J. D., Manteghi, N. A., Shouse, P. J., and Alves, W. J.: Soil Electrical Conductivity and Soil Salinity: New Formulations and Calibrations, Soil Science Society of America Journal, 53, 433–439, https://doi.org/https://doi.org/10.2136/sssaj1989.03615995005300020020x, 1989.

Rhoades, J. D., Chanduvi, F., and Lesh, S.: Soil Salinity Assessment-Methods and Interpretation of Electrical Conductivity Measurements. FAO Irrigation and Drainage paper No. 57, FAO, Rome, 1999.

Robinet, J., von Hebel, C., Govers, G., van der Kruk, J., Minella, J. P. G., Schlesner, A., Ameijeiras-Mariño, Y., and Vanderborght, J.: Spatial variability of soil water content and soil electrical conductivity across scales derived from

https://doi.org/10.5194/egusphere-2025-2696
Preprint. Discussion started: 25 June 2025

Electromagnetic Induction and Time Domain Reflectometry, Geoderma, 314, 160–174, https://doi.org/10.1016/j.geoderma.2017.10.045, 2018.

Robinson, D. A., Jones, S. B., Wraith, J. M., Or, D., and Friedman, S. P.: A Review of Advances in Dielectric and Electrical Conductivity Measurement in Soils Using Time Domain Reflectometry, Vadose Zone Journal, 2, 444–475, https://doi.org/https://doi.org/10.2136/vzj2003.4440, 2003.

Saeed, A., Comegna, A., Dragonetti, G., Lamaddalena, N., Sommella, A., and Coppola, A.: Soil electrical conductivity estimated by time domain reflectometry and electromagnetic induction sensors: Accounting for the different sensor observation volumes, Journal of Agricultural Engineering, 48, 223–234, https://doi.org/10.4081/jae.2017.716, 2017.

Sasaki, Y.: Full 3-D inversion of electromagnetic data on PC, J Appl Geophy, 46, 45–54, https://doi.org/https://doi.org/10.1016/S0926-9851(00)00038-0, 2001.

Selim, T., Bouksila, F., Berndtsson, R., and Persson, M.: Soil Water and Salinity Distribution under Different Treatments of Drip Irrigation, Soil Science Society of America Journal, 77, 1144–1156, https://doi.org/10.2136/sssaj2012.0304, 2013.

Serrano, J. M., Shahidian, S., and da Silva, J. R. M.: Apparent electrical conductivity in dry versus wet soil conditions in a shallow soil, Precis Agric, 14, 99–114, https://doi.org/10.1007/s11119-012-9281-6, 2013.

Shanahan, P. W., Binley, A., Whalley, W. R., and Watts, C. W.: The Use of Electromagnetic Induction to Monitor Changes in Soil Moisture Profiles beneath Different Wheat Genotypes, Soil Science Society of America Journal, 79, 459–466, https://doi.org/10.2136/sssaj2014.09.0360, 2015.

Sudduth, K. A., Kitchen, N. R., Wiebold, W. J., Batchelor, W. D., Bollero, G. A., Bullock, D. G., Clay, D. E., Palm, H. L., Pierce, F. J., Schuler, R. T., and Thelen, K. D.: Relating apparent electrical conductivity to soil properties across the north-central USA, Comput Electron Agric, 46, 263–283, https://doi.org/https://doi.org/10.1016/j.compag.2004.11.010, 2005.

Tlig, W., Mokh, F. El, Autovino, D., Iovino, M., and Nagaz, K.: Carrot productivity and its physiological response to irrigation methods and regimes in arid regions, Water Supply, 23, 5093–5105, https://doi.org/10.2166/ws.2023.304, 2023.

Topp, G. C., Davis, J. L., and Annan, A. P.: Electromagnetic Determination of Soil Water Content: Measurements in Coaxial Transmission Lines, Water Resour Res, 16, 574–582, https://doi.org/https://doi.org/10.1029/WR016i003p00574, 1980.

Western, A. W. and Blöschl, G.: On the spatial scaling of soil moisture, J Hydrol (Amst), 217, 203–224, https://doi.org/https://doi.org/10.1016/S0022-1694(98)00232-7, 1999.